Dissipation by a crystallization process

2016 EPL 113 10004

(http://iopscience.iop.org/0295-5075/113/1/10004)

A Letters Journal Exploring the Frontiers of Physics

January 2016

EPL, **113** (2016) 10004 www.epljournal.org
doi: 10.1209/0295-5075/113/10004

Dissipation by a crystallization process

Sven Dorosz[1], Thomas Voigtmann[2,3] and Tanja Schilling[1]
[1] *Physics and Materials Science Research Unit, Université du Luxembourg - L-1511 Luxembourg, Luxembourg*
[2] *Institut für Materialphysik im Weltraum, Deutsches Zentrum für Luft- und Raumfahrt (DLR) D-51170 Köln, Germany*
[3] *Department of Physics, Heinrich-Heine-Universität Düsseldorf - D-40225 Düsseldorf, Germany*

received 12 October 2015; accepted in final form 8 January 2016
published online 28 January 2016

PACS 05.70.Ln – Nonequilibrium and irreversible thermodynamics
PACS 64.70.dm – General theory of the solid-liquid transition
PACS 64.60.qe – General theory and computer simulations of nucleation

Abstract – We discuss crystallization as a non-equilibrium process. In a system of hard spheres under compression at a constant rate, we quantify the amount of heat that is dissipated during the crystallization process. We interpret the dissipation as arising from the resistance of the system against phase transformation. An intrinsic compression rate is identified that separates a quasi-static regime from one of rapidly driven crystallization. In the latter regime the system crystallizes more easily, because new relaxation channels are opened, at the cost of forming a higher fraction of non-equilibrium crystal structures. We rationalize the change in the crystallization mechanism by analogy with shear thinning, in terms of a kinetic competition between near-equilibrium relaxation and external driving.

Crystallization from the metastable fluid is a non-equilibrium process. Yet, it is usually discussed in terms of quasi-equilibrium concepts such as transition state theory [1,2]. Those approaches do not account for the fact that any irreversible process of finite duration is inevitably subject to dissipation. Here, we present a numerical approach to quantify this dissipation for a system that crystallizes under compression. For slow compression rates, the dissipation is proportional to the driving rate, allowing us to identify an intrinsic resistance of the system to phase transformation. Above a certain compression rate, the response becomes a nonlinear function of the external driving. Crystallization in this regime proceeds faster, due to the opening of non-equilibrium relaxation channels.

A standard way to characterize irreversible processes is to quantify entropy production [3,4]. However, to do so directly is unpractical even for very simple model systems. Since we compress the system at a constant rate, we can bypass this problem: We evaluate the overall work performed on the system, and subtract the known equilibrium contribution.

As a model system we use hard spheres, the most simple system that shows a liquid-to-crystal transition [5]. Hard spheres are expected to capture the essential dynamical processes in dense liquids, since these are governed by excluded volume between the constituents [6,7]. Our results should thus be applicable to crystallization in many metallic systems as well as dense colloidal suspensions. Crystallization dynamics in hard spheres has been extensively studied in computer simulation and analysed using equilibrium concepts [8–12].

We perform standard Monte Carlo (MC) computer simulations of hard spheres in the NPT ensemble. The diameter of the spheres σ, the free diffusion time t_0, and the thermal energy k_BT define the units of length, time, and energy. The system is prepared in a fluid equilibrium state at constant pressure and then compressed with constant rate $\dot{P}$ for a duration τ. Under these conditions the work W performed on the system is given by $\mathrm{d}W = V(t)\dot{P}\,\mathrm{d}t$, where $V(t)$ is the volume response of the system to the external driving $\dot{P}$. After subtraction of the equilibrium Gibbs free-energy difference ΔG between the initial and final state, the dissipated energy associated to each simulation trajectory remains,

$$W_{\mathrm{diss}} = \int_0^\tau \dot{P}V(t)\,\mathrm{d}t - \Delta G. \tag{1}$$

The volume evolution of two typical trajectories is shown in fig. 1 (solid lines). Dashed lines indicate the equations of state of the liquid [13] and the crystal [14] used to evaluate ΔG. The dissipated energy W_{diss}, indicated by the shaded areas, consists of three contributions: (I) is the work associated with compression of the metastable liquid phase until the nucleation event occurs

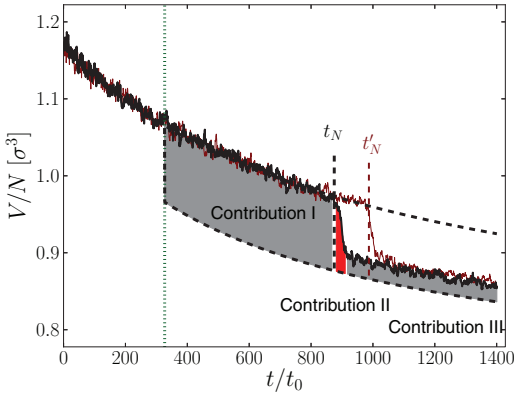

Fig. 1: (Colour online) Specific volume $V(t)/N$ along two typical simulation trajectories of a hard-sphere system compressed with a rate $\dot{P} = 0.01065\, k_BT/\sigma^3 t_0$ (solid lines). Induction times are labeled t_N and t'_N. Dashed lines indicate the equation of state of the metastable fluid (upper line) and the ideal equilibrium crystal (lower line). A vertical line marks the coexistence point. Shaded areas indicate the different contributions to the dissipated energy, eq. (1). Area (II) is the dissipation q^c during the crystallization process.

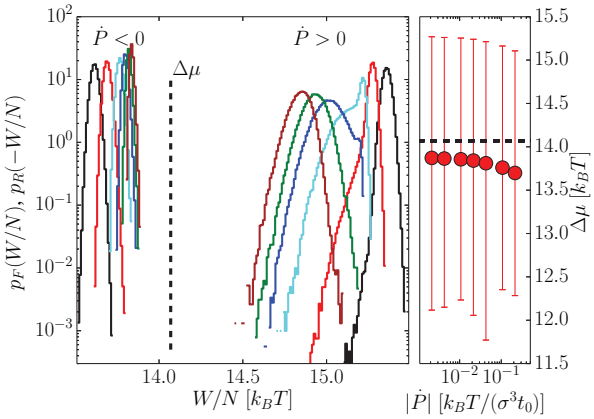

Fig. 2: (Colour online) Left panel: distribution of work per particle, $p(W/N)$, performed upon compression (forward process: right set of curves) and expansion (reverse process: left set of curves, shown as $p(-W/N)$) across the phase transition with a constant rate $|\dot{P}|$. Histograms are shown for $|\dot{P}| = 0.214, 0.107, 0.0428, 0.0214, 0.0107, 0.00428\, k_BT/\sigma^3 t_0$ (from right to left for the forward process). The dashed vertical line indicates the equilibrium chemical potential difference $\Delta\mu$. Right panel: $\Delta\mu$ estimated using the Jarzynski relation, eq. (3), see text. The horizontal dashed line indicates the equilibrium value.

at some induction time t_N. (III) is a contribution that arises because the system is not completely transformed into the equilibrium crystal during the simulation time, but contains defects. Its effect on the following analysis is minor. (I) and (III) are quasi-equilibrium contributions to $W_{\rm diss}$. Contribution (II) yields the non-equilibrium dissipation q^c associated with the crystallization process

$$q^c = \frac{1}{N}\int_{t_N}^{t_N+\Delta t} {\rm d}t\, \dot{P}\,[V - V_{\rm eq}(P)], \qquad (2)$$

where Δt is the process duration.

We briefly summarize the technical details of the MC simulation. Particle displacements are drawn from a flat distribution over $[-\Delta, \Delta]$ with $\Delta = 0.065\sigma$. As unit of time we use $t_0 = \sigma^2/D_0$, where the free-particle diffusion coefficient is $D_0 = \Delta^2/6$/MC sweep $\approx 7 \times 10^{-4}\sigma^2$/MC sweep. To control the pressure, a volume change is attempted once per MC sweep by rescaling the box lengths according to $L_i \mapsto L_i \exp[0.0012(r - 1/2)]$, where r is a uniform random variable in $]0, 1]$ and i labels the Cartesian directions. We allow changes of L_i independently in each direction to accomodate crystals with unit cells of different aspect ratios. Simulations start from an equilibrium fluid state at pressure $P_0 = 8\, k_BT/\sigma^3$ and end at $P_\tau = 23\, k_BT/\sigma^3$. (The crystal-liquid coexistence pressure is $P_c = 11.54\, k_BT/\sigma^3$ [15].) Trajectory durations $\tau = (P_\tau - P_0)/|\dot{P}|$ were chosen as $\tau = 1 \times 10^5$, 2×10^5, 5×10^5, 1×10^6, 2×10^6, 5×10^6, and 1×10^7 MC sweeps (corresponding to compression rates between $\dot{P} \approx 0.214\, k_BT/\sigma^3 t_0$ and $\dot{P} \approx 0.00214\, k_BT/\sigma^3 t_0$). We monitor the degree of crystallinity through the local $q_6 q_6$ bond order parameter [16,17] and analyze the averaged $|q_4|$ and $|q_6|$ to distinguish different crystal structures [18].

To compute q^c, eq. (2), we need to define the time window of the crystallization process, Δt. We set the induction time t_N to the time after which the largest crystalline cluster maintains a size of ten or more particles. The end of the process, $t_N + \Delta t$, is set to the time when the overall crystallinity reaches 60%. This value is large enough to capture the main contributions of dissipated heat, but still small enough to minimize the influence of periodic boundary conditions.

Since rare trajectories can contribute considerably to the non-equilibrium work distribution, we need to generate a very large number of independent trajectories ($O(10^5)$ runs for each compression rate). To reduce computational effort, we simulate a relatively small system of $N = 540$ particles. We have checked that this system is large enough to reproduce the nucleation rates obtained from simulations with $N = 8000$ and $N = 216000$ particles [19]. For each value of $\dot{P}$, we have sampled between 70000 and 650000 trajectories, obtained by selecting only those runs that crystallized to a degree of at least 75%. In total this required 90 years of CPU time on 2.2 GHz Xeons. In addition, to test for finite-size effects, we computed $\langle q^c \rangle$ for four different $\dot{P}$ with $N = 8000$ particles. As the simulation times would have become forbiddingly long when applying a barostat that simply rescales the particle positions, we used the barostat introduced by Almarza [20] instead. All results that we discuss in the following were qualitatively the same for the larger system, but due to the different choice of barostat the absolute values of the energies differed.

The distribution of total work per particle performed along the non-equilibrium trajectories is shown in fig. 2

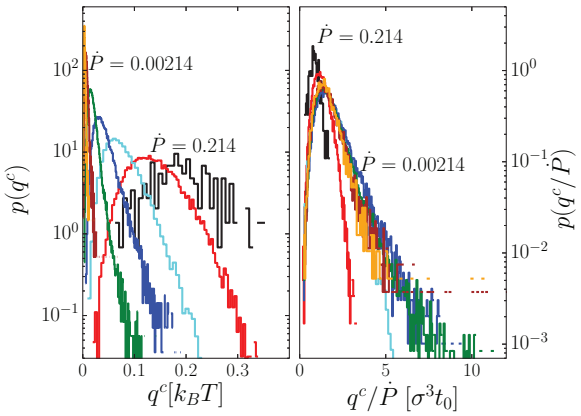

Fig. 3: (Colour online) Left panel: probability distribution of dissipated energy per particle during crystallization, q^c, for different compression rates, $\dot{P} = 0.00214, 0.0107, 0.0214, 0.0428, 0.107, 0.214\, k_BT/\sigma^3 t_0$, as indicated. Right panel: corresponding distributions of the crystallization loss, $q^c/\dot{P}$.

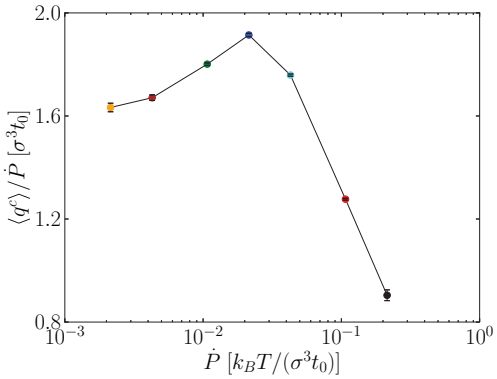

Fig. 4: (Colour online) Crystallization loss, *i.e.* the average energy per particle dissipated during crystallization relative to the external driving rate, $\zeta(\dot{P}) = \langle q^c \rangle / \dot{P}$, as a function of compression rate $\dot{P}$ (full symbols, with lines to guide the eye).

(left panel) for different $|\dot{P}|$. Upon compression ($\dot{P} > 0$), the distributions $p_{\rm F}(W/N)$ of this (forward) process are centered around values $W/N > \Delta\mu = \Delta G/N$. For small $\dot{P}$, the curves are monomodal and well described by Gaussian probability distribution functions down to the accuracy set by the number of trajectories that we simulated. The same is true upon expansion ($\dot{P} < 0$) for the (reverse) process involving melting, at all values of $|\dot{P}|$ considered here (shown in fig. 2 as $p_{\rm R}(-W/N)$). At larger $\dot{P}$, a more subtle structure is seen for the forward process. In particular around $\dot{P} \approx 0.0428\, k_BT/\sigma^3 t_0$, two distinct contributions to $p_{\rm F}(W/N)$ can be discerned.

The work distributions $p(W)$ of an arbitrary non-equilibrium process are connected to the equilibrium ΔG by fluctuation theorems [4]. Crooks' theorem [21] relates $p_{\rm F}(W)$ to $p_{\rm R}(W)$ by

$$p_{\rm F}(W) e^{-\beta W} = p_{\rm R}(-W) e^{-\beta \Delta G}, \qquad (3)$$

and integrating over W, one obtains the Jarzynski relation [22]. We use eq. (3) to test whether our $p(W)$ are consistent with the known ΔG. A direct test would require to sample both $p_{\rm F}(W)$ and $p_{\rm R}(-W)$ at $|W| \approx \Delta G$ well enough, but this is unfeasible with our current computational resources. To nevertheless get an estimate, we fit $p_{\rm F}(W)$ by a superposition of two Gaussians (although it need not be Gaussian in the tails), using eq. (3) with the data for $p_{\rm R}(-W)$ as a constraint. The values of $\Delta\mu$ estimated from this procedure are shown in fig. 2 (right panel, circles with error bars). They agree reasonably well with the known equilibrium $\Delta\mu$. This holds in particular also for the case where two distinct contributions can be discerned in the forward process.

The dissipation per particle q^c associated with the crystallization process is obtained after subtracting the equilibrium and quasi-equilibrium contributions from W/N. The left panel of fig. 3 shows the distribution $p(q^c)$ for various values of the compression rate $\dot{P}$. As the compression rate increases, the distribution shifts to higher average $\langle q^c \rangle$ and broadens. At the highest compression rate we simulated, $\langle q^c \rangle$ is about $0.2\, k_BT$, which is of the same order of magnitude as the average (macroscopic) interfacial energy over the area per particle, $\gamma\sigma^2 \approx 0.6\, k_BT$ [23]. For small $\dot{P}$, the distributions collapse when plotted in terms of the reduced variable $q^c/\dot{P}$, cf. fig. 3 (right panel). This collapse defines the regime of quasi-static behavior, where the response $q^c/\dot{P}$ of the system is independent of the driving force.

In the context of equilibrium thermodynamics the term "quasi-static" is restricted to the case of infinitely slow driving, $\dot{P} = 0$. The existence of a regime of $\dot{P}$-independent distributions of $q^c/\dot{P}$ justifies the extension of this notion to finite (small) driving rates. The limiting value of the average response $\zeta := \langle q^c \rangle / \dot{P}$ attained for $\dot{P} \to 0$ can be interpreted as an immanent system property, the *quasi-static crystallization loss*.

At driving forces above a threshold $\dot{P}^*$ the crystallization loss $\zeta(\dot{P})$ drops sharply with increasing $\dot{P}$, as shown in fig. 4. This marks the cross-over from the quasi-static to a strongly driven regime of crystallization.

Intuitively, one would expect the relative dissipation to increase once the rate of driving exceeds typical microscopic relaxation times of the system, as additional work can be dissipated through the microscopic degrees of freedom. The counterintuitive behavior of the crystallization loss can be rationalized by analogy with mechanical friction in fluids. There, one typically observes friction to decrease strongly in the nonlinear-response regime of fast driving [24]. This is particularly well known for the viscosity of non-Newtonian fluids [25], where the effect is called shear thinning. It also holds for a driven tracer subject to an external force in a dense fluid [26]. In these cases, the slow near-equilibrium relaxation processes are replaced by faster ones that occur on the time scale set by the external driving. In analogy, we interpret $\zeta(\dot{P})$ as a generalized friction coefficient that characterizes the resistance of the melt to phase transformation.

$\zeta(\dot{P})$ shows non-monotonic behavior because both effects, *i.e.*, increased friction through enhanced coupling to microscopic degrees of freedom as well as decreased friction through non-equilibrium relaxation channels, contribute to the crystallization loss. As indicated in fig. 3, the initial increase is associated with an increase in the large-q^c tail. This is intuitively expected since an increased coupling to microscopic degrees of freedom increases the probability for strongly dissipating trajectories. At $\dot{P} > \dot{P}^*$, this large-q^c tail is cut off. (We will show in the following that this effect is due to the formation of metastable crystal structures.) The cross-over between the two trends occurs around $\dot{P}^* \approx 2 \times 10^{-2}\, k_B T/\sigma^3 t_0$ (where the shape of $p(W)$ changes, as noted in connection with fig. 2). The cross-over value can be related to the time scale t_L needed for collective particle rearrangements involving the nearest and next-to-nearest neighbour shells. t_L is set by the long-time self-diffusion coefficient $D_L = \sigma^2/t_L$. For the typical densities reached when crystallization sets in, $D_L/D_0 = O(10^{-2})$ (for the initial fluid state in our work, $D_L/D_0 \approx 0.04$) [27]. Hence, $\dot{P}^* t_L = O(k_B T/\sigma^3)$; *i.e.* the effects of the external driving start to dominate the crystallization process once the compression rate is faster than the typical thermal energy density can be redistributed through collective particle rearrangements.

In constant-volume simulations of crystallization starting from over-compressed hard-sphere fluid states [9,10], the time scale t_L was also identified as determining the induction times t_N, as long as the initial packing fraction was smaller than $\phi \approx \phi_g = 0.58$ (corresponding to $V/N \approx \pi\sigma^3/6\phi \approx 0.903$). Above this packing fraction, $t_N \ll t_L$ was found; hence, two regimes of nucleation were identified, based on equilibrium concepts (termed nucleation-and-growth and spinodal nucleation). The distinction between two regimes of crystallization that we discuss here, based on a cross-over to far-from-equilibrium response, is fundamentally different. Note that for $\dot{P} \approx \dot{P}^*$, our simulations reach an average packing fraction at t_N of $\phi \approx 0.55 < \phi_g$, thus there is not even a coincidence in the packing fractions at cross-over for these different phenomena.

In the strongly driven regime, $\dot{P} > \dot{P}^*$, the melt relaxes faster into the crystal phase than it does in the quasi-static case. This is seen in fig. 5 (left panel), where we show the distributions of the crystallization-process durations Δt. For small $\dot{P}$, the distributions collapse to a $\dot{P}$-independent curve with a pronounced tail at large Δt and an average $\langle \Delta t \rangle \approx 20 t_0 \approx t_L$. This confirms that long-time self-diffusion sets the relevant time scale for the crystallization process in the quasi-static regime. At large $\dot{P}$, the large-Δt tail is cut off and $p(\Delta t)$ narrows with increasing $\dot{P}$. This suggests that the external driving rate sets a relevant time scale, $(k_B T/\sigma^3)/\dot{P}$, for the crystallization process at $\dot{P} > \dot{P}^*$.

This accelerated crystallization mechanism proceeds through non-equilibrium relaxation channels, in particular the formation of metastable crystal structures (bcc instead of fcc). The right panel of fig. 5 shows the probability distribution of the fraction of particles with a bcc-like environment in the crystal at the end of the simulation run. Again, at slow driving rates, $\dot{P} \lesssim \dot{P}^*$, the distributions are independent of $\dot{P}$. For $\dot{P} \gtrsim \dot{P}^*$, the formation of bcc structures is facilitated strongly. There even is a significant number of runs that crystallize completely into bcc. Interestingly, the question why fcc is the stable equilibrium structure while bcc should form more easily is known from Landau theory [28]. There, the effect arises because a larger set of reciprocal lattice vectors is needed to form fcc. This implies that a larger set of local density fluctuations needs to be sampled. It is plausible that this takes more time, and hence, bcc is favored kinetically at large driving rate $\dot{P}$.

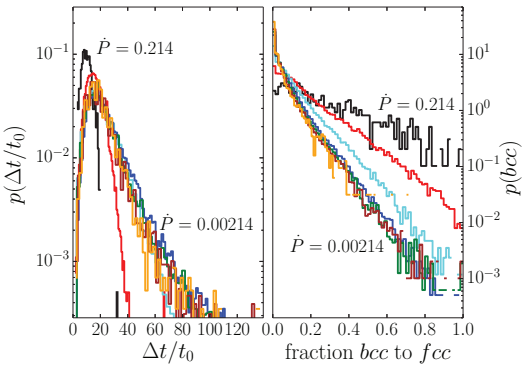

Fig. 5: (Colour online) Left: distribution of the time interval Δt over which the system crystallizes, for different $\dot{P}$ corresponding to the data shown in fig. 3. For the two highest values of $\dot{P}$, vertical lines indicate the maximum Δt that would be possible for the earliest induction time t_N observed. Right: distribution of the fraction of bcc crystal structures in the crystalline part of the system at the end of the compression run.

The tendency to form metastable crystal structures in rapid solidification is well known from metallic melts [29] and also colloidal suspensions [30]. It is often attributed to Ostwald's step rule, which invokes interfacial tensions between the crystal nucleus and the surrounding fluid [17]. These are inherently equilibrium, macroscale quantities that might not be well defined for a non-equilibrium process and on the scale of a few particle diameters. In particular since the dissipation along the process can be of the same order of magnitude as the interfacial energy, an explanation of the appearance of metastable structures on the basis of kinetic processes (as first indicated in ref. [31]) appears more reasonable.

In summary, we have discussed the crystallization process in terms of non-equilibrium notions. As a central quantity, we have calculated the distribution of heat dissipated during the process. Compressing the system at different rates $\dot{P}$ and measuring the volume response, we observe two regimes: that of near-equilibrium quasi-static crystallization below a characteristic compression rate $\dot{P}^*$, and the strongly driven far-from-equilibrium regime above. The cross-over $\dot{P}^*$ is set by the time scale

of collective particle rearrangements and the coexistence pressure. This cross-over is analogous to the one from linear response to nonlinear response in driven fluids, and extends the notion of these regimes to the dynamics across the first-order phase transition. Below $\dot{P}^*$, the resistance of the system against the phase transition, $\zeta(\dot{P}) = \langle q^c \rangle / \dot{P}$, is constant, and the system responds quasi-statically. Above $\dot{P}^*$ the crystallization process is facilitated, because new relaxation channels are opened via the formation of bcc structures instead of the thermodynamically favored fcc ones.

* * *

This project has been financially supported by the National Research Fund Luxembourg under the project FRPTECD. Computer simulations presented in this paper were carried out using the HPC facilities of University of Luxembourg [32]. We thank M. Allen, J. Horbach, and S. Williams for useful discussions.

REFERENCES

[1] Kashchiev D. and Rosmalen G. M. V., *Cryst. Res. Technol.*, **38** (2003) 555.
[2] Oxtoby D. W., *Adv. Chem. Phys.*, **70** (2009) 263.
[3] Evans D. J. and Morriss G. P., *Statistical Mechanics of Nonequilibrium Liquids* (Cambridge University Press, Cambridge, UK) 2008.
[4] Seifert U., *Rep. Prog. Phys.*, **75** (2012) 126001.
[5] Alder B. J. and Wainwright T. E., *J. Chem. Phys.*, **27** (1957) 1208.
[6] Widom B., *Science*, **157** (1967) 365.
[7] Voigtmann Th., *Phys. Rev. Lett.*, **101** (2008) 095701.
[8] Zaccarelli E., Valeriani C., Sanz E., Poon W. C. K., Cates M. E. and Pusey P. N., *Phys. Rev. Lett.*, **103** (2009) 135704.
[9] Pusey P. N., Zaccarelli E., Valeriani C., Sanz E., Poon W. C. K. and Cates M. E., *Philos. Trans. R. Soc. London, Ser. A*, **367** (2009) 4993.
[10] Valeriani C., Sanz E., Zaccarelli E., Poon W. C. K., Cates M. E. and Pusey P. N., *J. Phys.: Condens. Matter*, **23** (2011) 194117.
[11] Sanz E., Valeriani C., Zaccarelli E., Poon W. C. K., Pusey P. N. and Cates M. E., *Phys. Rev. Lett.*, **106** (2011) 215701.
[12] Taffs J., Williams S. R., Tanaka H. and Royall C. P., *Soft Matter*, **9** (2013) 297.
[13] Carnahan N. F. and Starling K. E., *J. Chem. Phys.*, **51** (1969) 635.
[14] Alder B. J., Hoover W. G. and Young D. A., *J. Chem. Phys.*, **49** (1968) 3688.
[15] Noya E. G., Vega C. and de Miguel E., *J. Chem. Phys.*, **128** (2008).
[16] Steinhardt P., Nelson D. and Ronchetti M., *Phys. Rev. B*, **28** (1983) 784.
[17] ten Wolde P. R., Ruiz-Montero M. J. and Frenkel D., *Phys. Rev. Lett.*, **75** (1995) 2714.
[18] Lechner W. and Dellago C., *J. Chem. Phys.*, **129** (2008).
[19] Schilling T., Dorosz S., Schöpe H. J. and Opletal G., *J. Phys.: Condens. Matter*, **23** (2011) 194120.
[20] Almarza N. G., *J. Chem. Phys.*, **130** (2009) 184106.
[21] Crooks G. E., *Phys. Rev. E*, **60** (1999) 2721.
[22] Jarzynski C., *Phys. Rev. Lett.*, **78** (1997) 2690.
[23] Härtel A., Oettel M., Rozas R. E., Egelhaaf S. U., Horbach J. and Löwen H., *Phys. Rev. Lett.*, **108** (2012) 226101.
[24] Urbakh M., Klafter J., Gourdon D. and Israelachvili J., *Nature*, **430** (2004) 525.
[25] Voigtmann Th., *Curr. Opin. Colloid Interface Sci.*, **19** (2014) 549.
[26] Puertas A. M. and Voigtmann Th., *J. Phys.: Condens. Matter*, **26** (2014) 243101.
[27] Alder B. J., Gass D. M. and Wainwright T. E., *J. Chem. Phys.*, **53** (1970) 3813.
[28] Alexander S. and McTague J., *Phys. Rev. Lett.*, **41** (1978) 41.
[29] Herlach D. M., *Metals*, **4** (2014) 196.
[30] Zhou H., Xu S., Sun Z., Du X. and Liu L., *Langmuir*, **27** (2011) 7439.
[31] O'Malley B. and Snook I., *Phys. Rev. Lett.*, **90** (2003) 085702.
[32] Varrette S., Bouvry P., Cartiaux H. and Georgatos F., *Management of an Academic HPC Cluster: The UL Experience*, presented at *Proceedings of the 2014 International Conference on High Performance Computing & Simulation (HPCS 2014)* (IEEE, Bologna, Italy) 2014.